UNIVERSIDADE ESTADUAL PAULISTA
"JULIO DE MESQUITA FILHO"
INSTITUTO DE GEOCIÊNCIAS E CIÊNCIAS EXATAS

Trabalho de Conclusão de Curso

Curso de Graduação em Física

ON THE VERSATILITY OF THE ISING MODEL AND ITS APPLICATIONS

Matheus Henrique De Matos Ramos

Prof. Dr. Mariano de Souza

Rio Claro (SP)

2024

UNIVERSIDADE ESTADUAL PAULISTA

Instituto de Geociências e Ciências Exatas

Câmpus de Rio Claro

Matheus Henrique de Matos Ramos

ON THE VERSATILITY OF THE ISING MODEL AND ITS APPLICATIONS

Trabalho de Conclusão de Curso apresentado ao Instituto de Geociências e Ciências Exatas - Câmpus de Rio Claro, da Universidade Estadual Paulista Júlio de Mesquita Filho, para obtenção do grau de Bacharel e Licenciado em Física.

Rio Claro - SP

2024

R175t

Ramos, Matheus Henrique de Matos
On the versatility of the Ising model and its applications / Matheus Henrique de Matos Ramos. -- Rio Claro, 2024
30 p. : il.

Trabalho de conclusão de curso (Bacharelado e licenciatura - Física) - Universidade Estadual Paulista (UNESP), Instituto de Geociências e Ciências Exatas, Rio Claro
Orientador: Mariano de Souza

1. Modelo de Ising. 2. Célula Compressiva. 3. Água Super-resfriada. 4. Isolantes de Mott. 5. COVID-19. I. Título.

Sistema de geração automática de fichas catalográficas da Unesp. Dados fornecidos pelo autor(a).

Matheus Henrique de Matos Ramos

ON THE VERSATILITY OF THE ISING MODEL AND ITS APPLICATIONS

Trabalho de Conclusão de Curso apresentado ao Instituto de Geociências e Ciências Exatas - Câmpus de Rio Claro, da Universidade Estadual Paulista Júlio de Mesquita Filho, para obtenção do grau de Bacharel e Licenciatura em Física.

Comissão Examinadora

Prof. Dr. Mariano de Souza

Prof. Dr. Andriano José Galvani Otuka

Prof. Dr. Carlos Cezar Bof Bufon

Rio Claro, 19 de Novembro de 2024.

Assinatura do aluno

Assinatura do orientador

Acknowledgements

I would like to thank Professor Mariano de Souza for accepting to be my advisor, for showing me the path in the search for truth, and for guiding me academically, contributing to my personal growth. I especially thank Lucas Cezar Gomes Squillante for his valuable advice and all the members of the Solid State group of Rio Claro.

I also want to thank my family for giving me life, emotional and financial support, especially my mother, Sandra Gonçalves de Matos Ramos, my father, Marcelo Aparecido Santos Ramos, and my second mother, Damiana Silva dos Santos. I want to deeply thank my partner, Paloma do Prado Santiago, for providing emotional support during this final stretch of my degree.

I express my gratitude to the friends made along this journey, to the class I joined in 2018, and to my housemates from Vacalhada and Curral. All of you hold a special place in my heart. Thank you, everyone! And finally, I thank my dog, Candy, for showing me that life also needs affection and love!

I, Matheus Henrique de Matos Ramos, declare that every word in the text of my submitted work is solely my responsibility. I acknowledge that my advisor bears no responsibility for any potential errors or inaccuracies within this document.

Signed,

Matheus Henrique de Matos Ramos,

2/12/2024

Abstract

This work addresses Ising-type models, originating from Wilhelm Lenz's initial contributions in 1920 and formalized by Ernst Ising in his 1924 doctoral thesis, where he described the behavior of ferromagnetic materials. These models were developed to represent interactions between nearest-neighbor spins in a linear chain, forming a simplified yet rich system for describing significant physical phenomena. The solutions to these models allow for the calculation of various thermodynamic properties of the system under study, providing clear insight into system behavior during phase transitions. Despite its simplicity, Ising initially considered the model a "toy" and abandoned its use, with its applications taking years to be fully explored. Today, Ising-type models transcend the bounds of physics, with interdisciplinary applications in fields such as economics, biology, medicine, and even in predicting electoral outcomes.

This monograph aims to review and discuss these applications, based on a comprehensive physical and mathematical analysis of the 1-D Ising model to highlight the versatility of these models. To this end, solutions to the 1-D Ising model will be presented, along with an approach to the compressible-cell model. This in-depth understanding will enable a more critical analysis of the applications of these models in various contexts, from predicting critical phenomena in physical systems to understanding complex biological processes.

Throughout this work, cases of Ising model applications in diverse areas, such as supercooled water and Mott metal-to-insulator transitions, will be examined. Through this analysis, the study will demonstrate how the Ising model, initially conceived as a simple tool in physics, has become essential in various scientific and social disciplines, underscoring its remarkable versatility and contemporary relevance.

Keywords: Ising Model, Compressive cell, Supercooled Water, Mott Insulators, COVID-19

Resumo

O presente trabalho aborda modelos do tipo Ising, originados a partir das contribuições iniciais de Wilhelm Lenz em 1920 e formalizados por Ernst Ising em sua tese de doutorado de 1924, na qual ele descreveu o comportamento de materiais ferromagnéticos. Estes modelos foram concebidos para representar as interações entre primeiros vizinhos em uma cadeia linear de spins, constituindo um sistema simplificado, porém rico na descrição de fenômenos físicos relevantes. A solução desses modelos permite o cálculo de diversas grandezas termodinâmicas do sistema em estudo, possibilitando uma compreensão clara do comportamento do sistema na proximidade da região de transições de fase. Apesar de sua simplicidade, Ising inicialmente considerou o modelo um "brinquedo"e abandonou sua utilização. Suas aplicações, porém, levaram anos para serem plenamente exploradas. Hoje, os modelos do tipo Ising transcendem os limites da física, com aplicações interdisciplinares em áreas como economia, biologia, medicina e até na previsão de resultados eleitorais.

Esta monografia tem como objetivo revisar e discutir aplicações, fundamentando-se em uma revisão física e matemática abrangente do modelo 1-D para evidenciar a versatilidade desses modelos. Para alcançar esse objetivo, serão apresentadas soluções do modelo Ising em 1D, além de uma sutil abordagem do modelo da célula compressiva. Esse entendimento aprofundado permitirá uma análise mais criteriosa das aplicações dos modelos em diferentes contextos, desde a predição de fenômenos críticos em sistemas físicos até a compreensão de fenômenos biológicos complexos.

Ao longo deste trabalho, serão examinados casos de aplicação dos modelos do tipo Ising em diversas áreas, como no estudo da água superresfriada e nas transições de Mott de metal para isolante. Através dessa análise, será possível evidenciar como o modelo Ising, inicialmente concebido como ferramenta simples na física, torna-se fundamental em diversas disciplinas científicas e sociais, demonstrando sua notável versatilidade e relevância contemporânea.

Palavras-chave: Modelo de Ising, Célula Compressiva, Água Super-resfriada, Isolantes de Mott, COVID-19

Table of contents

1 Introduction

The Ising model has been studied in the last few decades; the model has a versatile characteristic to describe the region alloy in the transition phase, providing the exact solution for first-neighbor interaction. Important to study materials that have the attributes of ferromagnetic and paramagnetic, where there are unpaired electron interactions. The initial idea consists of a chain of an electron with spin $S = +\frac{1}{2}(-\frac{1}{2})$, and each electron interacts with the nearest neighbor and could interact with an external magnetic field. For a 1-D chain, there exists an exact solution for this system [1]; for the 2-D chain, there exists a numerical solution for many cases [2]; and for a 3-D chain, there is no analytic solution, which is investigated nowadays in literature.

It is possible to assume that the physical system can be represented by a regular lattice arrangement of molecules in space. We are interested in three kinds of physical systems: (1) Magnets, in which each molecular has a spin that can be oriented either up or down, which can be relative to the direction of an externally applied field; (2) Mixtures of two kinds of molecule; (3) Mixture of molecules and "hole"(empty spaces) [3]. Depending on whether this variable has the value $+1$ or -1, we say that the molecular at that node (1) has spin up, or spin down, (2) belongs to one or the other of two species, or (3) is present or absent [3].

Usually, the two-value variable is called the spin σ_i, associates with site i of the lattice. A lattice configuration is a particular set of values of all the spins; if N nodes exist, there will be 2^N different configurations. Assume that interaction energy depends only on the configuration of neighboring nodes of the lattice. In the three types of physical systems mentioned above, such an interaction could lead to (1) spontaneous magnetization, with all or most spin in the same direction even in the absence of an external field; (2) phase separation, the molecule of the same kind clustering together; (3) condensation of molecules into one region of space, leaving space in the rest of the container [3].

In this study, we used the Ising model, which considers a spin chain, and the compressive cell model to expand on ideas about the model. The analyzed studies were proposed by the advisor and aim to strengthen the understanding of the model and its applications. Accordingly, this work is organized as follows:

- Chapter 2: Detailed solution of the 1-D thermodynamical Ising model.
- Chapter 3: Explore the Ising model for energy volume and its application for the

supercooled water and metal-insulator Mott transition, and discuss the employment of the Ising model for epidemic spread, especially for COVID-19.

- Chapter 4: Conclusion and perspectives.

2 1-D thermodynamical Ising model

This chapter is dedicated to solution of the 1-D dimensional ising model discursing the detail of the diagonalization of the Hamiltonian. Making using the Krammer method of matrix transfor to diagonalize, to find the eingenergie, the free energy, and derivate thermodynamics such as the entropy, specfic heat, and magnetization [4, 5].

2.1 1-D Ising model solution

The Ising model has been studied for a few decades because it is possible to find the exact solution for interaction between the nearest-neighbors [4]. To figure out the solution for 1-D Ising model, let's consider a lattice of N sites with spins $\sigma_i = +1/2(-1/2)$ interacting with the nearest neighbor, as shows Fig. 1, in an open line, the Nth spin will miss the interaction with the *N+1* [4]. To ordering this, we define $\sigma_1 = \sigma_{N+1}$, which means the last spin of the lattice interact with the first spin [4, 5]. This condition enables us to transform the open line in a curved chain without lose the linear property, so this configures can be described by the Hamiltonian [4]:

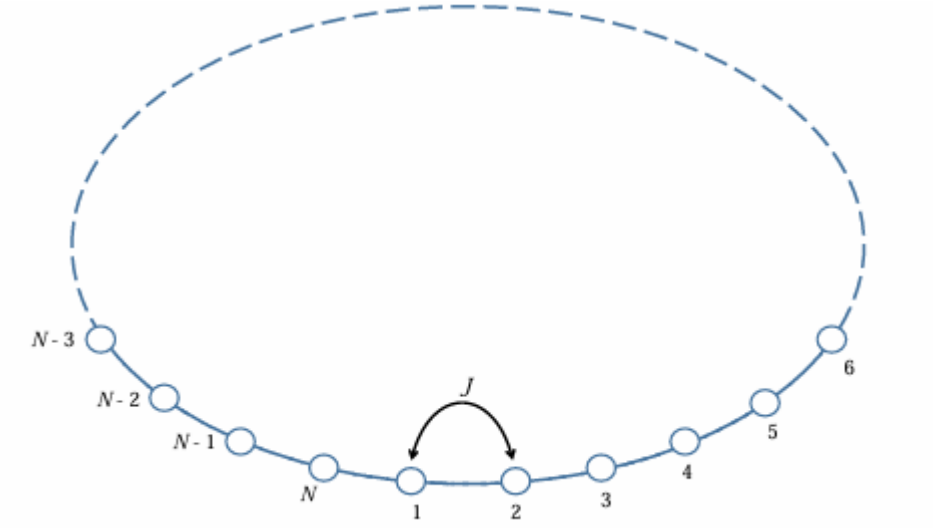

Fig. 1 – Ising closed infinite chain where each small circle represents a spin, J represents the coupling constant between the spins . Figure extracted from Ref. [5], [4].

$$H\{\sigma_i\} = \underbrace{-J\sum_{i,j}^{N}\sigma_i\sigma_j}_{\text{(i)}} \underbrace{-\mu_B B\sum_{i=1}^{N}\sigma_i}_{\text{(ii)}}, \tag{2.1}$$

the J term is the couple energy interaction between spins σ_i with σ_j, σ_j refer to the neighbors, B is the external magnetic field, and μ_B is Bohr magneton [4]. The part (i)

and (ii) of Eq. 2.1 represent, respectively, the energy interaction between spins and the energy interaction between the spin σ_i with the external magnetic field [4, 5]. Analyzing separately the case without an external field, considering only the part (i) of Eq. 2.1. The complete solution considers those two parts of the Hamiltonian. To proceed with the solution, the partition function must be determined to obtain the thermodynamic observables of this configuration system. So consider the partition function [4]:

$$Z(T,B) = \sum_{\sigma_1=\pm 1}^{N} e^{-\beta H}. \tag{2.2}$$

First, we can start the diagonalization considering that the case where the Hamiltonian H is consistent only by H_i, meaning there is only interaction between the spin neighbors and no external field applied. So insert the H_i in Eq. 2.2:

$$\begin{aligned} Z_i(T,0) &= \sum_{\sigma_1=\pm 1}^{N} e^{-\beta H_i}, \\ &= \sum_{\sigma_1=\pm 1}^{N} e^{\beta J \sum_{i,j}^{N} \sigma_i \sigma_j}. \end{aligned} \tag{2.3}$$

Note that the properties of exponential $e^{a+b} = e^a e^b$. This permit writing the partition function, Eq. 2.3, as the sum of an exponential production. An important consideration is the neighbor spin σ_j can be rewritten as σ_{i+1} because in 1-D case there is only interaction with previous and next nears neighbors [4, 5]. The Eq. 2.3 turns:

$$\begin{aligned} Z_{(i)}(T,0) &= \sum_{\sigma_1=\pm 1}^{N} exp(\beta J \sum_{i+1}^{N} \sigma_i \sigma_{i+1}), \\ &= \sum_{\sigma_1=\pm 1}^{N} e^{\beta J \sigma_1 \sigma_2} \times e^{\beta J \sigma_2 \sigma_3} \times \cdots \times e^{\beta J \sigma_N \sigma_1}. \end{aligned} \tag{2.4}$$

Note that there are only four probability configurations for those interactions. These configurations can be described as a function of a matrix transfer $\mathbf{T}(\sigma_i, \sigma_{i+1}) = e^{(\beta J \sigma_i \sigma_{i+1})}$, where the operator matrix is described by:

$$T = \begin{pmatrix} \langle \uparrow | \mathbf{T} | \uparrow \rangle & \langle \uparrow | \mathbf{T} | \downarrow \rangle \\ \langle \downarrow | \mathbf{T} | \uparrow \rangle & \langle \downarrow | \mathbf{T} | \downarrow \rangle \end{pmatrix}. \tag{2.5}$$

Where those matrix elements are:

$$\begin{aligned} \langle \uparrow | \mathbf{T} | \uparrow \rangle &= e^{\beta [J.(+1).(+1)]} = e^{\beta J}, \\ \langle \uparrow | \mathbf{T} | \downarrow \rangle &= e^{\beta [J.(+1).(-1)]} = e^{-\beta J}, \\ \langle \downarrow | \mathbf{T} | \uparrow \rangle &= e^{\beta [J.(-1).(+1)]} = e^{-\beta J}, \\ \langle \downarrow | \mathbf{T} | \downarrow \rangle &= e^{\beta [J.(-1).(-1))]} = e^{\beta J}. \end{aligned} \tag{2.7}$$

Thus, Eq. 2.4 becomes:

$$Z_i(T,0) = \sum_{\sigma_1=\pm1} \cdots \sum_{\sigma_N=\pm1} \langle\sigma_1|\mathbf{T}|\sigma_2\rangle\langle\sigma_2|\mathbf{T}|\sigma_3 \cdots \langle\sigma_{N-1}|\mathbf{T}|\sigma_N\rangle\langle\sigma_N|\mathbf{T}|\sigma_1\rangle. \tag{2.8}$$

Since that it is a sum of a product of matrix, the partition function will be given by the eigenvalues of the operator matrix $\mathbf{T}$, which means $\mathrm{Tr}(T^N)$ [4]:

$$Z_i = \sum_{\sigma_i=\pm1} \langle\sigma_1|\mathbf{T}^N|\sigma_1\rangle = \mathrm{Tr}(\mathbf{T}^N) = \lambda_+^N + \lambda_-^N, \tag{2.9}$$

where the λ_+ and λ_- are the eingevalues of the operator matrix $\mathbf{T}$ [4]. Thus, the determinant to find the eigenvalue of $\mathbf{T}$, i.e., $\det|\mathbf{T} - \lambda\mathbf{I}| = 0$, becomes:

$$\begin{vmatrix} e^{\beta J} - \lambda & e^{-\beta J} \\ e^{-\beta J} & e^{\beta J} - \lambda \end{vmatrix} = 0, \tag{2.10}$$

$$(e^{\beta J} - \lambda)^2 - e^{-2\beta J} = 0, \tag{2.11}$$

$$\lambda^2 - 2e^{\beta J}\lambda + 2\sinh(2\beta J) = 0. \tag{2.12}$$

Find the value of λ in Eq. 2.12, using the Bhaskara formula (i.e $ax^2 + bx + c = 0 \rightarrow x_\pm = \dfrac{-b \pm \sqrt{b^2 - 4ac}}{2a}$); note $a = 1, b = 2e^{\beta J}, c = sinh(2\beta J)$, so its follow as [5]:

$$\begin{aligned} \lambda_\pm &= \frac{2e^{\beta J} \pm \sqrt{4e^{2\beta J} - 8\sinh(2\beta J)}}{2} \\ &= e^{\beta J} \pm \sqrt{e^{2\beta J}(1 - \frac{2\sinh(2\beta J)}{e^{2\beta J}})} \\ &= e^{\beta J} \pm e^{\beta J}\sqrt{e^{-4\beta J}} \end{aligned}$$

$$\boxed{\lambda_\pm = e^{\beta J} \pm e^{-\beta J}}. \tag{2.13}$$

which gives us the following solution to the eigenvalues of $\mathbf{T}$:

$$\lambda_+ = 2\cosh(\beta J), \quad \lambda_- = 2\sinh(\beta J). \tag{2.14}$$

Ploting those eigenvalue (Fig. 2), immediately note that for T finite the $\lambda_+ > \lambda$ and for $T \approx 0 \rightarrow \lambda_+ \approx \lambda_-$. So that inserting those eigenvalues on the Eq. 2.9, and considering only the λ_+, because since the $\lambda_+ > \lambda_-$ for finite T, implies $\lambda_+^N >> \lambda_-^N$, for N sufficiently big [4]. Thus:

$$Z_i = \lambda_+^N + \lambda_-^N \approx \lambda_+^N = [2\cosh(\beta J)]^N. \tag{2.15}$$

With this result, its possible to calculate the free energy Helmholtz (i.e $F = -k_B T \ln Z$):

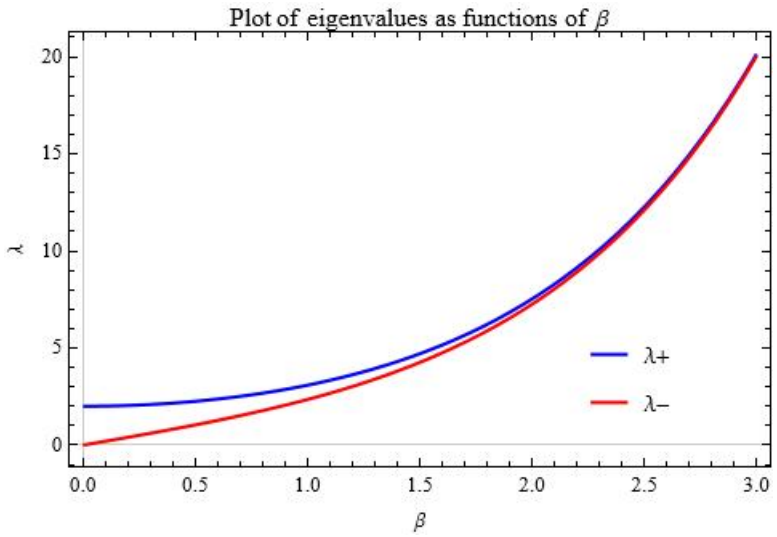

Fig. 2 – Plot of eigenvalues as function of β. Note, that the $\lambda_+ > \lambda_-$ for finite T, because the $\beta = 1/k_BT$, and when $T \to 0$, $\lambda_+ \approx \lambda_-$.

$$F(T,0) = -k_BT \ln Z = -k_BT \ln\{2\cosh(\beta J)\}^N = -Nk_BT \ln\{2\cosh(\beta J)\}. \tag{2.16}$$

The free energy per particle is given by $f_0(T) = \dfrac{F}{N}$, the subindices indicate the absence of external field, thus:

$$\boxed{f_0(T) = -k_BT \ln\{2\cosh(\beta J)\}}. \tag{2.17}$$

Thus, it's possible to calculate the non-external field entropy, and the specific heat as follows [4]:

- Entropy

$$S_0 = -\frac{df_0(T)}{dT} = k_B \ln\{2\cosh\left(\frac{J}{k_BT}\right)\} - \frac{J}{T}\tanh\left(\frac{J}{k_BT}\right). \tag{2.18}$$

- Specific Heat

$$C_0 = -T\frac{d^2f_0(T)}{dT^2} = Nk(\beta J)^2 \mathrm{sech}^2(\beta J). \tag{2.19}$$

From the entropy, Eq. 3, it is possible to infer the behavior of the entropy at the zero fields, with the increase of temperature the entropy converges to k_Bln2, as an expected to a two-state system, because the thermal fluctuations induce the transition between states, and for the $T \to 0$ the system become an ordering system [4,6]. The specific heat at zero-field is given by Eq. 2.19, and Fig. 4. That for $T = 0$ $C_0 \to 0$, because the

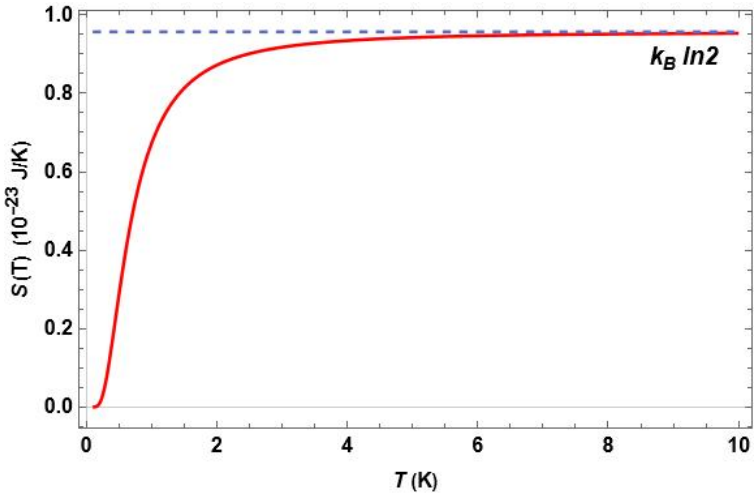

Fig. 3 – Illustrate the entropy behavior to a 1-D Ising model, for $T \to 0$, $S_0 \to 0$. It occurs because the system becomes an ordinary system and with the increase of the temperature the entropy converges to $k_B \ln 2$, because there are only 2 states for the system to occupy [6, 7].

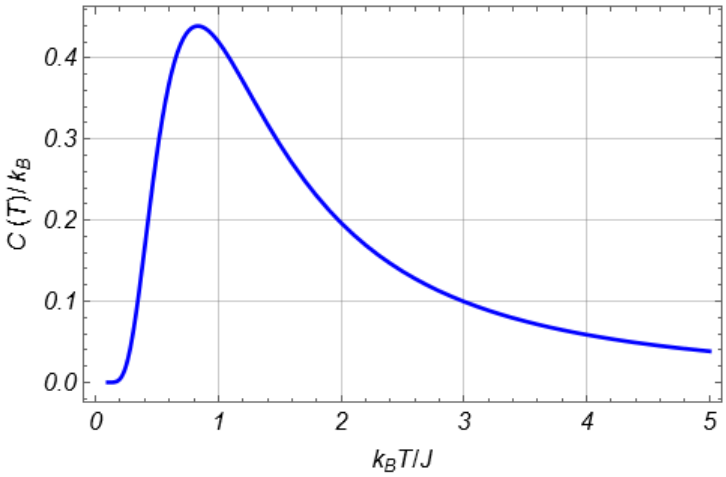

Fig. 4 – The zero-field specific heat of an Ising chain as a function of temperature. The maximum point represents the Schottky anomalies, where the thermal energy and the energy couple are equivalent, then the thermal energy can induce a transition between the two states [7].

thermal energy is not enough to change the entropy of the system. The maximum refers to the *Schottky anomalies*, which mean in at this point the temperature as more probability to induce excitations between states, the specific heat became smooth with the increase of the temperature converging to the classical Dulong-Petit specific heat, because with increase of temperature the excitations between states saturate [7].

Return to the complete Hamiltonian (Eq. 2.1), and considering $j = i+1$ is the next nearest neighbor, its possible rewrite as:

$$H_N\{\sigma_i\} = -J\sum_{i=1}^{N}\sigma_i\sigma_{i+1} - \frac{1}{2}\mu_B B\sum_{i=1}^{N}(\sigma_i + \sigma_{i+1}). \tag{2.20}$$

Doing the same process of Eq. 2.20, is possible to diagonalize the Hamiltonian, using the partition function $Z_N(T, B)$ as:

$$Z_N(T,B) = \sum_{\sigma_1=\pm1} \cdots \sum_{\sigma_N=\pm1} e^{-\beta J \sum_{i=1}^{N} \sigma_i\sigma_{i+1} - \frac{1}{2}\mu_B B \sum_{i=1}^{N}(\sigma_i+\sigma_{i+1})}$$
$$= \sum_{\sigma_1=\pm1} e^{-\beta J\sigma_1\sigma_2 - \frac{1}{2}\mu_B B(\sigma_1+\sigma_2)} \times \cdots \times e^{-\beta J\sigma_N\sigma_1 - \frac{1}{2}\mu_B B(\sigma_N+\sigma_1)}. \tag{2.21}$$

By defining the operator matrix T, as:

$$\langle\sigma_i|\mathbf{T}|\sigma_{i+1}\rangle = \exp\{-\beta J\sigma_i\sigma_{i+1} - \frac{1}{2}\mu_B B(\sigma_i+\sigma_{i+1})\}. \tag{2.22}$$

Eq. 2.21, becomes:

$$Z_N(T,B) = \sum_{\sigma_1=\pm1} \cdots \sum_{\sigma_N=\pm1} \langle\sigma_1|\mathbf{T}|\sigma_2\rangle\langle\sigma_2|\mathbf{T}|\sigma_3\rangle \cdots \langle\sigma_{N-1}|\mathbf{T}|\sigma_N\rangle\langle\sigma_N|\mathbf{T}|\sigma_1\rangle. \tag{2.23}$$

Now, to calculate the element of the operator matrix:

$$\mathbf{T} = \begin{pmatrix} \langle\uparrow|\mathbf{T}|\uparrow\rangle & \langle\uparrow|\mathbf{T}|\downarrow\rangle \\ \langle\downarrow|\mathbf{T}|\uparrow\rangle & \langle\downarrow|\mathbf{T}|\downarrow\rangle \end{pmatrix}. \tag{2.24}$$

where:

$$\langle\uparrow|\mathbf{T}|\uparrow\rangle = e^{\beta[J.(+1).(+1)+\frac{1}{2}\mu_B B(1+1)} = e^{\beta(J+\mu_B B)},$$
$$\langle\uparrow|\mathbf{T}|\downarrow\rangle = e^{\beta[J.(+1).(-1)+\frac{1}{2}\mu_B B(1-1)} = e^{-\beta J},$$
$$\langle\downarrow|\mathbf{T}|\uparrow\rangle = e^{\beta[J.(-1).(+1)+\frac{1}{2}\mu_B B(-1+1)} = e^{-\beta J},$$
$$\langle\downarrow|\mathbf{T}|\downarrow\rangle = e^{\beta[J.(-1).(-1)+\frac{1}{2}\mu_B B(-1-1)} = e^{\beta(J-\mu_B B)}.$$

The matrix $\mathbf{T}$ becomes:

$$\mathbf{T} = \begin{pmatrix} e^{\beta[J+\mu_B B]} & e^{-\beta J} \\ e^{-\beta J} & e^{\beta[J-\mu_B B]} \end{pmatrix}. \tag{2.25}$$

So, the Eq. 2.21 turns a sum of a matrix product:

$$Z_N(T,B) = \sum_{\sigma_{\pm1}} \langle\sigma_1|\mathbf{T}^N|\sigma_1\rangle = Tr(\mathbf{T}^N) = \lambda_+^N + \lambda_-^N, \tag{2.26}$$

where λ_+ and λ_- are the eigenvalues of $\mathbf{T}$, evaluating the $\det|\mathbf{T}-\lambda\mathbf{I}| = 0$, result:

$$\det|\mathbf{T}-\lambda\mathbf{I}| = \begin{vmatrix} e^{\beta(J+\mu_B B)} - \lambda & e^{-\beta J} \\ e^{-\beta J} & e^{\beta(J-\mu_B B)} - \lambda \end{vmatrix} = 0, \tag{2.27}$$

$$[0e^{\beta(J+\mu_B B)} - \lambda][e^{\beta(J-\mu_B B)} - \lambda] - (e^{-\beta J})(e^{-\beta J}) = 0,$$
$$\lambda^2 + e^{2\beta J} - e^{-2\beta J} - \lambda[e^{\beta(J-\mu_B B)} + e^{-\beta(-J+\mu_B B)}] = 0,$$
$$\lambda^2 + 2.e^{\beta J}\cosh(\beta\mu_B B) + 2\sinh(2\beta J) = 0. \tag{2.28}$$

Solving Eq. 2.28 for λ:

$$\lambda_{\pm} = \frac{2e^{\beta J}\cosh(\beta\mu_B B) \pm \{4e^{2\beta J}\cosh^2(\beta\mu_B B) - 8\sinh(2\beta J)\}^{\frac{1}{2}}}{2},$$
$$\lambda_{\pm} = 2e^{\beta J}\cosh(\beta\mu_B B) \pm 2\{e^{2\beta J}[1+\sinh^2(\beta\mu_B B)] - [e^{2\beta J)} - e^{-2\beta J}]\}^{\frac{1}{2}},$$
$$\lambda_{\pm} = e^{\beta J}\cosh(\beta\mu_B B) \pm \{[e^{2\beta J} + e^{2\beta J}\sinh^2(\beta\mu_B B)] - [e^{2\beta J)} - e^{-2\beta J}]\}^{\frac{1}{2}},$$
$$\lambda_{\pm} = e^{\beta J}\cosh(\beta\mu_B B) \pm \{e^{2\beta J}\sinh^2(\beta\mu_B B)] + e^{-2\beta J}\}^{\frac{1}{2}}.$$

$$\lambda_{\pm} = e^{\beta J}\left(\cosh(\beta\mu_B B) \pm \sqrt{\sinh^2(\beta\mu_B B) + e^{-4\beta J}}\right). \tag{2.29}$$

where $\lambda_+ > \lambda-$, because the square root term is positive for any value of T [4]. When $N \to \infty$ it is considered only the λ_+ eigenvalue alone, since λ_- is small when compared with λ_+ in the thermodynamic limit [4]. Thus, the partition function from Eq. 2.21 becomes [4]:

$$Z_N(T,B) = \lambda_+^N. \tag{2.30}$$

The Helmholtz free energy is given by [6]:

$$F(T,B) = -k_B T \ln[Z_N(T,B)]. \tag{2.31}$$

Thus, inserting Eq. 2.30 into Eq. 2.31:

$$\begin{aligned} F(T,B) &= -k_B T \ln\left(\lambda_+^N\right) = -k_B T N \ln\left(\lambda_+\right) \\ &= -k_B T N \ln[e^{\beta J}\left(\cosh(\beta\mu_B B) + \sqrt{\sinh^2(\beta\mu_B B) + e^{-4\beta J}}\right)] \\ &= -k_B T N \beta J - k_B T N \ln\left(\cosh(\beta\mu_B B) + \sqrt{\sinh^2(\beta\mu_B B) + e^{-4\beta J}}\right). \end{aligned}$$

$$F(T,B) = -k_B T N \beta J - k_B T N \ln\left(\cosh(\beta\mu_B B) + \sqrt{\sinh^2(\beta\mu_B B) + e^{-4\beta J}}\right). \tag{2.32}$$

Thus, the free energy $F(T,B)$ is given by:

$$\boxed{F(T,B) = -N\left\{J + k_B T N \ln\left(\cosh(\beta\mu_B B) + \sqrt{\sinh^2(\beta\mu_B B)] + e^{-4\beta J}}\right)\right\}.} \tag{2.33}$$

Thus, the free energy per spin [4, 5]:

$$f(T,B) = \frac{F(T,B)}{N}, \tag{2.34}$$

Resulting:

$$f(T,B) = -J - k_B T \ln\left(\cosh(\beta\mu_B B) + \sqrt{e^{-4\beta J} + \sinh^2(\beta\mu_B B)}\right). \tag{2.35}$$

From Eq. 2.35, it is possible to derive all the thermodynamic physical quantities such as internal energy per particle U, entropy S, specific heat C, magnetization M, and magnetic susceptibility χ [4,6]. The total energy per particle of this system is given by [4]:

$$U = -\frac{1}{N}\left(\frac{\partial Z}{\partial \beta}\right)_B = f - T\left(\frac{\partial f}{\partial T}\right)_B. \tag{2.36}$$

Thus:

$$U = J + \frac{\mu_B B \sinh(\beta\mu_B B)}{\cosh(\beta\mu_B B) + \sqrt{\sinh^2(\beta\mu_B B) + e^{-4\beta J}}} \tag{2.37}$$

$$+ \frac{\sinh(\beta\mu_B B)\mu_B B\cosh(\beta\mu_B B) - 2Je^{-4\beta J}}{\left(\cosh(\beta\mu_B B) + \sqrt{\sinh^2(\beta\mu_B B) + e^{-4\beta J}}\right)\sqrt{\sinh^2(\beta\mu_B B) + e^{-4\beta J}}}. \tag{2.38}$$

The magnetization of this system is given by [4,6,7]:

$$M(T,B) = -\left(\frac{\partial f(T,B)}{\partial B}\right)_T. \tag{2.39}$$

This give us:

$$M(T,B) = -\frac{\partial}{\partial B}(-J - k_B T \ln[\cosh(\beta\mu_B B) + \sqrt{e^{-4\beta J} + \sinh^2(\beta\mu_B B)})$$

$$= k_B T \frac{\beta\mu_B \sinh(\beta\mu_B B) + \frac{1}{2}\frac{2\beta\mu_B \sinh(\beta\mu BB)\cosh(\beta\mu_B B)}{\sqrt{e^{-4\beta J}+\sinh^2(\beta\mu_B B)}}}{\cosh(\beta\mu_B B) + \sqrt{e^{-4\beta J} + \sinh^2(\beta\mu_B B)}}.$$

$$\boxed{M(T,B) = -\mu_B \frac{\sinh(\beta\mu_B B)}{\sqrt{\sinh^2(\beta\mu_B B) + exp(-4J\beta)}}}. \tag{2.40}$$

This expression for magnetization enables us to calculate the magnetic susceptibility. Note, by the Fig. 5, the behavior of this equation shown that for $B \to 0$, $\overline{M} \to 0$ for all finite T value [4]. This rules out the possibility of spontaneous magnetization, and hence of a phase transition [4]. Also, when the term $J\beta = 0$, essentially we have the paramagnetic result $\overline{M} = \mu tanh(\beta\mu B)$ [4,7]. A positive J enhances magnetization and, in turn, leads to a faster approach toward saturation. As $T \to 0$, the magnetization curves become a step function - indicative of a singularity at $T = 0$ [4]. The susceptibility expression is calculated as $\chi(T,B) = (\partial M(B,T)/\partial B)_T$, as follows:

$$\chi(T,B) = \frac{\mu_B\beta\cosh(\beta\mu_B B)(-\mu_B\sqrt{\sinh^2(\beta\mu_B B) + e^{-4J\beta}} + \sinh^2(\beta\mu_B B)}{(\sinh^2(\beta\mu_B B) + e^{-4J\beta})^{3/2}}. \tag{2.41}$$

The low-field susceptibility of the system is given by the initial slope of the magnetization curve; one obtains which implies that the zero field the susceptibility is given by [4]:

$$\chi_0(T) = \frac{\mu^2}{k_B T}e^{2J/k_B T}. \tag{2.42}$$

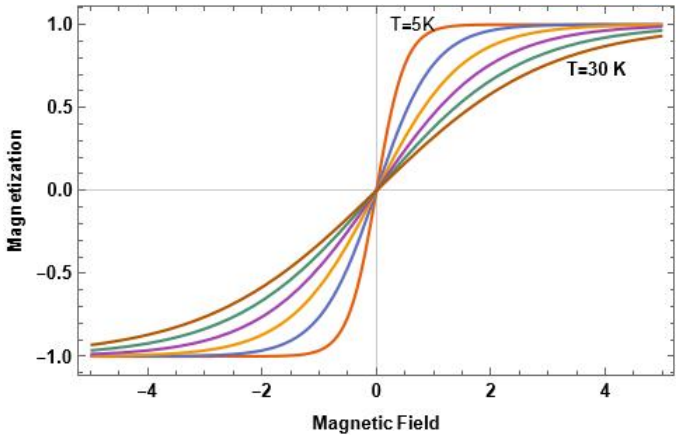

Fig. 5 – Plot of magnetization *versus* external magnetic field. The lines represent different values of constant of coupling and temperature. When $T \to 0$, the magnetization expression tends to a step function [4].

The entropy is calculated by Eq. 2.18. Thus, applying the Eq. 2.35 in Eq. 2.18:

$$
\begin{aligned}
S(T,B) &= -\left(\frac{\partial f(T,B)}{\partial T}\right)_B \\
&= -\left(\frac{\partial(-J - k_B T \ln[\cosh(\beta\mu_B B) + \{e^{-4\beta J} + \sinh^2(\beta\mu_B B)\}^{\frac{1}{2}}])}{\partial T}\right)_B,
\end{aligned}
$$

$$
\begin{aligned}
S(T,B) =& k_B ln(cosh(\beta\mu_B B) + \sqrt{sinh^2(\beta\mu_B B) + e^{-4J\beta}}) + \\
&+ \frac{2J}{T}\frac{e^{-4J\beta}}{(cosh(\beta\mu_B B) + \sqrt{sinh^2(\beta\mu_B B) + e^{-4J\beta}})\sqrt{sinh^2(\beta\mu_B B) + e^{-4J\beta}}} + \\
&- \frac{\mu_B B}{T}\frac{sinh(\beta\mu_B B))}{\sqrt{sinh^2(\beta\mu_B B) + exp(-4J\beta)}}.
\end{aligned}
\tag{2.43}
$$

The entropy with the magnetic field is analogous to the entropy at zero-field. Fig. 6 shows the entropy curves for different values of the magnetic field, demonstrating the influence of the magnetic in keeping the lattice in the ordering phase when the thermal energy increase [6]. The curves converge to saturation value $k_B \ln 2$ as except to the system with two possible states [6].

With the entropy depicted in Fig. 6, it is possible to explore the process of adiabatic demagnetization cooling. This technique involves initially applying a magnetic field to reduce the system's entropy. Subsequently, by decreasing the applied magnetic field and pressure, the system's temperature can be lowered, as illustrated in Fig. 7. The adiabatic process is important to keep the same entropy after reduce the applied magnetic field and as the consequence reduce the temperature of the system [6, 7]. The limit of this process associate to the intrinsic intrinsic local magnetic field of electron [8].

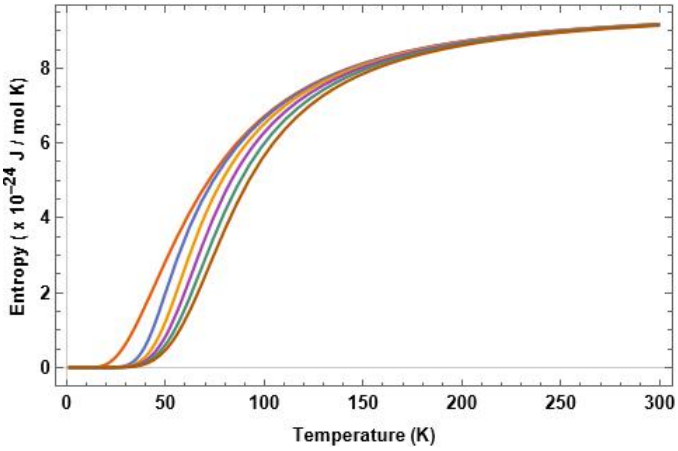

Fig. 6 – Entropy vs temperature to different value of the magnetic field. The top curve refer to a low magnetic field, the increase of the magnetic field in entropy curve keep the ordering in for while the temperature increase until the thermal energy begins to promote new accessible states [6,7].

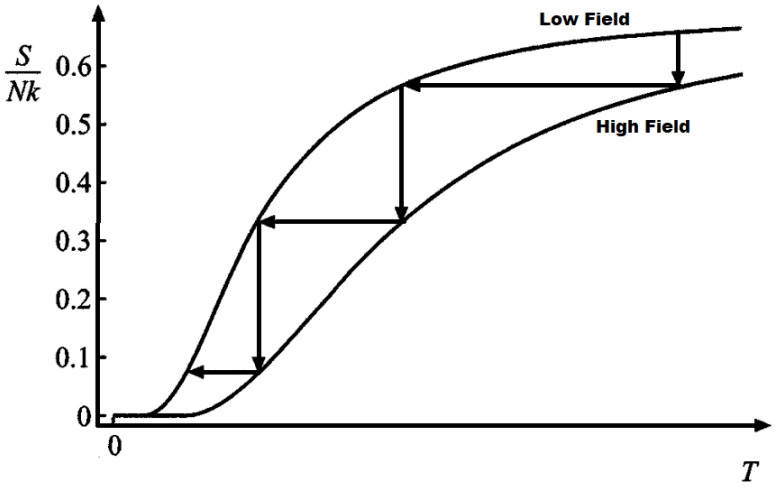

Fig. 7 – Schematic of the demagnetization cooling with the successive step of isothermal magnetization and adiabatic demagnetization [6, 7]. Extracted from Ref. [6].

3 Applications

In this section, we will discuss the fundamental applications of the Ising model, highlighting key aspects of the model and examining its results in various contexts. We will explore applications such as the compressible-cell Ising model for supercooled water, the Griffiths phase in the Mott metal-to-insulator transition, and the use of the Ising model to study epidemic spread dynamics. Each application demonstrates the versatility of the Ising model in capturing complex behaviors in different systems.

3.1 Ising-like model for compressible-cell and supercooled water

This section will explore the Ising-like models for energy-volume coupling in the frame of Ref. [9]. This method considers a rectangular lattice that N sites and each site is associated with a cell with a coordinate number c [9]. Each cell has two possible accessible volumes. Employing analogous properties of $S = +\frac{1}{2}(-\frac{1}{2})$ from the 1D thermodynamical Ising model [9]. For the volume $v_- = v_0$, and $v_+ = v_0 + \delta v$ [9]. This means there is a competition of two possible volumes in the cell. Thus, assuming $n_i = 1(0)$ to the $(+)$, $(-)$ volumes, and that each cell has a characteristic free volume for $0 < \dot{v}_+ < v_+$ and $0 < \dot{v}_- < v_-$, them the ratio of this characteristic volume move is given by $\lambda = \frac{\dot{v}_+}{\dot{v}_-}$ [9], as show in Fig. 8 . Thus, the energy and volume that describes this system configuration are given by [9]:

$$E\{n_i\} = \frac{c}{2} N\epsilon_0 - \delta\epsilon \sum_{i,j} n_i n_j, \tag{3.1}$$

and

$$V\{n_i\} = Nv_0 + \delta v \sum_{i=0}^{N} n_i, \tag{3.2}$$

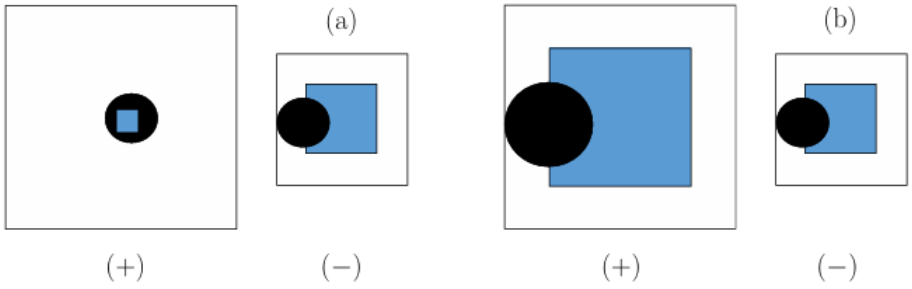

Fig. 8 – Single-cell (+) and (-) states for two situations, (a) and (b) [9]. The shaded (blue) areas are the free volumes a particle can explore in its cell [9]. In (a), it is considered that the free particle volume of a particle in (+) cells is restricted so that $\lambda < 1$. In (b), two particle sizes are used while $\lambda > 1$ [9]. Extracted from Ref. [9].

where E is the total energy of the system, $\delta\epsilon$ the energy interaction, and ϵ_0 the energy interaction between the volume. The N measures the total volume, and δv is the additional volume of the low-density molecule, for example water molecule. This energy configuration enables us to consider maximum energy occurs when all particles are v_-, resulting in $E_{max} = \frac{cN}{2}$. The minimal energy is given by $E_{min} = [cN\epsilon_0 - \delta(N-1)N]/2$ when the system dominated by v_+. Both minimal and maximum volume respectively $V_{min} = Nv_0$ and $V_{max} = N(v_0 + \delta v)$ [9].

Thus, examining the isothermal-isobaric ensemble for this system summing over the $e^{-\beta E}$ and $e^{-\beta pV}$ Boltzmann factor over microstate give us the partition function Z(N,p,T):

$$Z(N,p,T) = \sum_i^N \exp(-\beta E + \beta pV), \tag{3.3}$$

$$Z(N,p,T) = \sum_i^N exp(-\beta(\frac{c}{2}N\epsilon_0 - \delta\epsilon\sum_{i,j} n_i n_j) + \beta p(Nv_0 + \delta v\sum_i^N n_i), \tag{3.4}$$

$$= \sum_i^N \exp(-\beta(\frac{c}{2}N\epsilon_0 + pNv_0) exp(\beta(\delta\epsilon\sum_{i,j} n_i n_j - p\delta v\sum_i^N n_i),$$

$$Z(N,p,T) = exp(-\beta(\frac{c}{2}N\epsilon_0 + pNv_0)\sum_i^N exp(\beta(\delta\epsilon\sum_{i,j} n_i n_j - p\delta v\sum_i^N n_i). \tag{3.5}$$

Eq. 3.5 has the same structure as the canonical Ising model. However, here it has some difference of the 1D thermodynamical Ising model, such as it is a 3D Ising model, and involves isothermal-isobaric which difficult to find the analytical solution to this system [9]. The solution comes from the *Mean-field approximation*, make using the *saddle-point approximation*, it is possible to define the equation of states [9]. And from it derivate the thermodynamic observables as the specific heat, isothermal thermal expansion, and the value of the critical points as the critical temperature, critical pressure and critical volume [9]. This method as been crucial to study systems where there are liquid-liquid interaction as in supercooled water [9, 10], and explorer insight in case of Mott metal-insulator transition [10], and the protein compartmentalization [11].

3.1.1 Supercooled Water

Supercooled water is a phenomenon in which liquid water remains in a liquid state below its normal freezing point, often down to temperatures as low as under certain conditions. The concept of a liquid-liquid transition in supercooled water refers to the hypothesis that water might exist in two distinct liquid phases: a high-density liquid (HDL) and a low-density liquid (LDL) [12]. This anomaly is not directly related to the supercooled liquid-liquid transition but adds to water's unusual behavior that draws the attention of scientists in different area, such as meteorology, detecting clouds formation

with supercooled droplets [13]; and food engineer to food, in the context of freezing and preservation preservation [14]. As seen in the last subsection the recently proposed so-called compressive cell Ising-like model is a tool explaining the transition phase between liquid-liquid, considering the existence of high- and low-density [9, 10]. So, the model consists of a system with "N" sites and a coordination number c [9,10]; the c coordination is an adimensional constant responsible for expressing the influence of the interaction among the sites when compared to the intrinsic energy [10]. The $cN\epsilon_0/2$ gives the inherent energy system, where the N is the total of molecules in the system, and ϵ_0 is an arbitrary energy value [9]. Hence, it considers the high- and low-density, is essential to define the n_i, analogous to $S = +1/2(-1/2)$, that assumes value $n_i = 1$ to the volume $v0 + \delta v$, low density, and $n_i = 0$ to volume v_0, high-density [9]. Thus, to total energy is given by $E\{n_i\}$, where [9, 10]:

$$E\{n_i\} = \frac{cN\epsilon_0}{2} - \delta\epsilon \sum_{\langle i,j \rangle} n_i n_j. \tag{3.6}$$

As discussed in the previous subsection, the recently proposed compressive cell Ising-like model provides a framework for explaining the liquid-liquid phase transition, specifically accounting for high- and low-density liquid states [9, 10]. In this model, a system with N sites and coordination number c is used, where c is a dimensionless constant expressing the relative influence of interactions among sites compared to the system's intrinsic energy [10]. The term $\frac{cN\epsilon_0}{2}$ represents the inherent energy of the system, with N being the total number of molecules, and ϵ_0 an arbitrary energy reference [9].

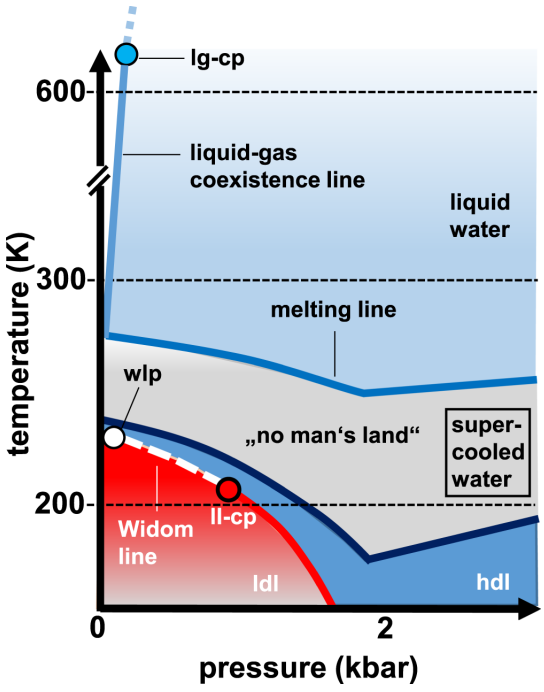

Fig. 9 – Water phase diagram, lg-cp refer to liquid-gas critical-point, wlp refer to the window line point, the red dot refer to the liquid-liquid critical point [10]. Both ldl and hdl are respectively the low density liquid, and high-density liquid [10]. Image extracted from Ref. [10].

Note if all molecules are in the high-density state, the maximum energy will be intrinsic energy $E_{max} = \frac{cN\epsilon_0}{2}$ [9]. For all molecular in the low-density state, the energy system is minimal because $E_{min} = \frac{cN\epsilon_0 - \delta\epsilon(N-1)N}{2}$ [9]. It is also possible to define the total volume of this system as [9, 10]:

$$V\{n_i\} = Nv_0 + \delta v \sum_{i=0}^{N} n_i. \tag{3.7}$$

The δv is the volume increment responsible for the additional volume of the low-density molecule [9, 10]. The maximum volume is $v_{max} = N(v_0 + \delta v)$, which means the low-density molecule occupies all cells, and the minimal volume is $V_{min} = Nv_0$ [9, 10]. Thus, to analyze this system configuration and observe its uses, the isothermal-isobaric ensemble, considering the partition function $Z(N, P, T) = \sum \exp(\beta E + \beta pV)$ [9, 10]. This partition function will result in an equation similar to the canonical Ising model partition function; the fundamental difference here lies in dimensions, for this model is considered a 3-D lattice, which means the model can not be calculated analytically [9]. Thus, it is necessary to recall the method of Mean-field to get a qualitative solution [9]. The solution provides results that can be used to calculate the Grünsaisen ratio of the supercooled water, which is essential to deeply understanding the behavior of supercooled water and analyzing the signature in the coexistence phase [10].

3.1.2 The Mott metal to insulator transition

The Mott metal-to-insulator transition is a significant topic of strongly correlated electron systems [15–17]. The Mott insulator emagers in dopped semiconductor, as the κ-(BEDT-TTF)X class material [17]. Unlike conventional insulators, which are defined by the classical band theory as materials with an empty or completed filled band, Mott insulators emerge from metallic phases, displaying insulating behavior under low pressure due to strong electron-electron interactions [15, 16]. In Mott insulators, the ratio of Coulomb repulsion, U, to the bandwidth, W, follows $U/W \propto p^{-1}$, where increasing Coulomb repulsion counteracts pressure [16]. This relationship exemplifies how Coulomb interactions can induce an insulating state even in systems with partially filled conduction bands [16, 17].

To examine this critical transition region, the autor in Ref. [17] consider a Griffiths phase where metallic and insulating "puddles"coexist. In this context the compressive cell Ising-like model was employed , as an analogy the spin-up $\sigma = 1/2$ represents insulating regions, while spin-down $\sigma = -1/2$ represents metallic regions, as illustrated in Fig. 10. Based on this definition, the quantities of metallic and insulating puddles can be determined by [17]:

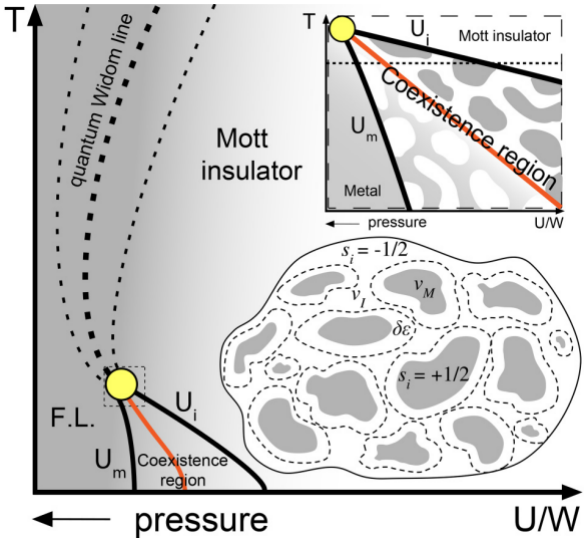

Fig. 10 – Main panel: Schematic phase diagram of temperature T versus $U/W \propto p^{-1}$ for κ-(BEDT-TTF)$_2$Cu$_2$(CN)$_3$ [17]. The diagram illustrates the coexistence region, the quantum Widom line, and the critical point (yellow dot) [17]. F.L. represents the Fermi-liquid phase [17]. The Metallic (U_m) and insulating (U_i) spinodal lines are shown, delimiting the phase coexistence region [17]. The solid orange line indicates the first-order transition [17]. Upper inset: Zoomed-in view of the coexistence region, with a cartoon of metallic puddles embedded within an insulating phase [17]. The horizontal dashed line shows a hypothetical sweep of U/W at constant temperature T/W [17]. Lower inset: Illustration of the proposed electronic Griffiths-like phase, where metallic puddles ($\sigma_i = +1/2$) with volume v_M are embedded in an insulating medium ($\sigma_i = -1/2$) with volume v_I, and the dash lines represent the interaction energy between the metallic puddle [17]. Figure extracted from Ref. [17].

$$N^M = \sum_i^N 2\left(\sigma_i + \frac{1}{2}\right)\sigma_i,$$

$$N^I = \sum_i^N 2\left(\sigma_i - \frac{1}{2}\right)\sigma_i,$$

where N^M and N^I denote the numbers of metallic and insulating puddles, respectively, and the total number of puddles is given by $N = N^M + N^I$ [10].

The total energy of the system can be expressed as [17]:

$$E^T(s_i) = N\epsilon_0 - \epsilon' \sum_{\langle i \neq j \rangle}^N \left[2\left(s_i + \frac{1}{2}\right)s_i\right] \times \left[2\left(s_j + \frac{1}{2}\right)\right],$$

where N is the total number of puddles, ϵ_0 represents the energy associated with insulating puddles, and ϵ' denotes the energy of metallic puddles [10].

This approach, grounded in mixed-phase theory, allows for the analysis of phase transition signatures in the Mott metal-to-insulator transition [17]. By accessing thermodynamic observables such as the free energy of the mixed phase, entropy, isothermal compressibility, and specific heat at a constant electric field, it is possible to gain insights

into the behavior of these materials [17]. Additionally, the magnetocaloric effect in this class of materials can be determined by the magnetic Grüneisen parameter [17].

3.2 The COVID-19 pandemics

In 2020, the world experienced the widespread impact of COVID-19, leading to prolonged lockdowns. During this time, the State Solid Physics group proposed using the Ising model to study the spread of infections, as documented in their paper [18]. By drawing an analogy between the Ising model and the susceptible infected recovered (SIR) model, they represented infected individuals and healthy individuals as spins in opposite states (up and down) [18]. This approach, combined with the logistic function to model infection dynamics, highlighted the critical role of quarantine in reducing transmission by limiting contact between infected and healthy individuals [18]. While not a real-time predictive model—owing to numerous factors like viral evolution and quarantine adherence—the Ising model effectively demonstrated the importance of isolation in curbing COVID-19 spread [18].

The model also considers environmental influences, suggesting that colder weather slows transmission, while warmer conditions might increase it [18]. By applying the Ising model to epidemic curves, this approach underscores the value of linking statistical physics and mathematical models to biological systems [18]. The Ising model offers conceptual clarity on disease dynamics.

Thus, using the Ising model in tandem with logistic distribution is beneficial for explaining the Gaussian-like distribution of infection curves and the effectiveness of quarantine measures [18]. In this model, a spin-$S = 1/2$ Ising system is adapted, with spin-up ($p_i = 1/2$) representing infected individuals and spin-down ($p_i = -1/2$) representing healthy individuals. The total infected population, N^+, is given by [18]:

$$N^+ = \sum_{i=1}^{N} 2\left(p_i + \frac{1}{2}\right) p_i, \tag{3.8}$$

while the healthy population, N^-, is represented similarly, where N denotes the total population. In the absence of interaction between two infected or two healthy individuals, the interaction energy $\delta\epsilon$ is zero [18]. However, for contacts between infected and healthy individuals (or vice versa), $\delta\epsilon \neq 0$ [18]. The total population C_T, which includes the effects of contact between infected and healthy individuals, can be described by the equation [18]:

$$C_T = C_h - 4\delta\epsilon \sum_{\langle i \neq j = 1 \rangle}^{N} \left[\left(\frac{1}{2} + p_i\right)\left(\frac{1}{2} - p_j\right) + \left(\frac{1}{2} - p_i\right)\left(\frac{1}{2} + p_j\right)\right] p_i p_j, \tag{3.9}$$

where C_h is the initial number of healthy individuals before the virus spread, and p_j represents the neighbor of p_i [18]. The second term on the right side of Eq. 3.9 is always negative when $p_i = 1/2$ and $p_j = -1/2$ (or vice versa) [18].

The interaction term $\delta\epsilon$ is associated with the number of individuals in quarantine, denoted as n, where $1 < n < N$. Considering $\delta\epsilon \propto n^{-1/2}$, this suggests that increasing the number of people in quarantine decreases the interaction between infected and healthy individuals, thus reducing the peak of the infection curve, as illustrated in Fig. 11. The model is robust because it is possible to considerate the weather influence, daily life contact, and possible reason of external contact [18]. The difficult of this model is to find the between the $\delta\epsilon \propto n^t$, find the exponent t is the challenge to make the right approximation [18]. The Fig. 12 shows the visualization of the quarantine to stop of virus quarentine. Since the infected people restritic the contact its cut the ramifications a Bethee tree impling in the stop of possible infection in a given city [18].

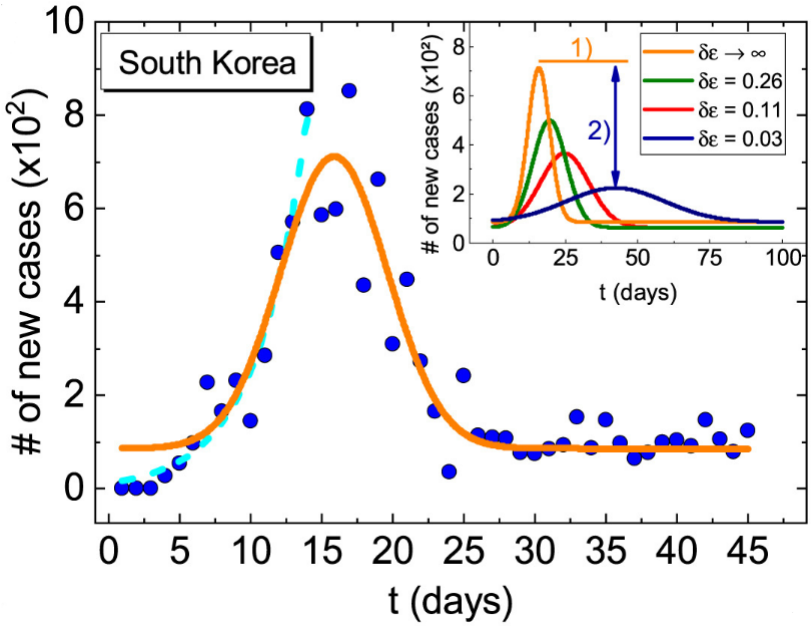

Fig. 11 – Main panel: The count of new infections in South Korea. The dashed line represents the predicted exponential spread, while the yellow line illustrates the Gaussian distribution fit [18]. The upper inset shows the different curve corresponding to energy interaction according to the number of people in quarantine [18]. Extracted from Ref. [18].

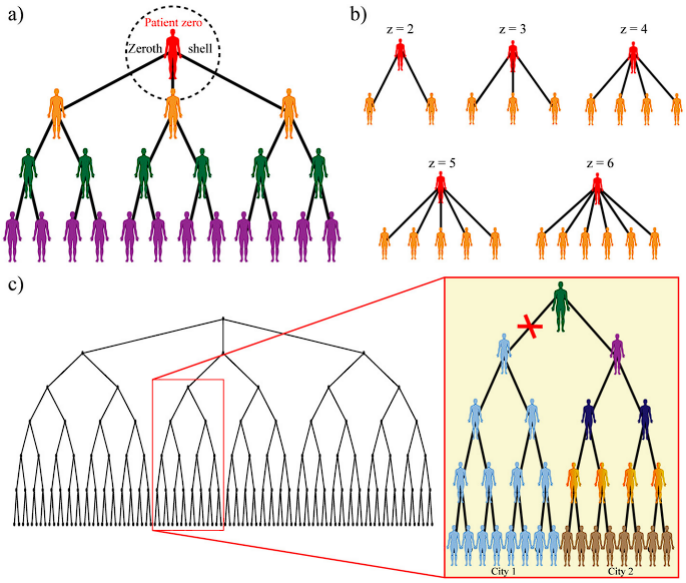

Fig. 12 – a) The patient zero has contact with tree individual, and the the next geration of contact with two order individuom, making a Bethe tree [18]. b) represention of the possible scenarios of start of dissemination [18]. c) Representation of the impact of quarantine on cut the ramification of Bethee tree [18]. Figure extracted from Ref. [18].

4 Conclusion and perspectives

This work explores the solution of the 1D Ising model, focusing on the derivation of thermodynamic observables and their graphical interpretations. Key concepts and applications are also addressed, including the compressible-cell model applied to supercooled water, the Mott metal-to-insulator transition, and the application of the Ising model to epidemic spread dynamics. The Ising model has been a robust method to describes phenomena in many areas, the limitations of the method is to find the interaction parameter appropriated to an accurate result.

Future work aims to further investigate concepts not covered here, such as mean-field approximations, experimental aspect of the supercooled water, and transition phases. Those effort will deepen the understanding of thermodynamic behavior and expand the exploration within experimental frameworks.

Refereces

1 E. Ising, Z. Phys. **31**, 253 (1925).

2 L. Onsager, Phys. Rev. **65**, 117 (1944).

3 S. G. Brush, Rev. Mod. Phys. **39**, 883 (1967).

4 R. K. Pathria, P. D. Beale, *Statistical Mechanics*, 3rd ed. Elsevier, Burlington, MA, (2011).

5 L. C. G. Squillante, *Investigation of Molecular Conductors, the Magneto–Caloric Effect* (Universidade Estadual Paulista, Instituto de Geociências e Ciências Exatas, Rio Claro, 2018), 76 pages, Orientador: V. P. M. de Souza.

6 R. Baierlein, *Thermal Physics* Cambridge University Press, Cambridge, (1999).

7 S. Blundell, *Magnetism in Condensed Matter*Oxford University Press, Oxford, (2001).

8 L. Squillante, I. F. Mello, G. O. Gomes, et al., Sci. Rep. **10**, 7981 (2020).

9 C. A. Cerdeiriña, H. E. Stanley, Phys. Rev. Lett. **120**, 120603 (2018).

10 O. Gomes, H.E. Stanley, M. de Souza, Sci. Rep. **9**, 12006 (2019).

11 L. Squillante, I. F. Mello, L. S. Ricco, M. F. Minicucci, A. M. Ukpong, A. C. Seridonio, R. E. Lagos–Monaco, M. de Souza, J. Cell. Phys. **10**, 15e34622 (2024).

12 L. Xu, P. Kumar, S. V. Buldyrev, S. H. Chen, P. H. Poole, F. Sciortino, H. E. Stanley, Proc. Natl. Acad. Sci. USA **102**, 16558 (2005).

13 G. Zhou, J. Wang, Y. Yin, X. Hu, H. Letu, B.–J. Sohn, Y. L. Yung, C. Liu, Geophys. Res. Lett. **49**, e2021GL096115 (2022).

14 G.G. Stonehouse, J.A. Evans, J. Food Eng. **148**, 74 (2015).

15 L. Bartosch, M. de Souza, M. Lang, Phys. Rev. Lett. **104**, 245701 (2010).

16 M. de Souza, L. Bartosch, J. Phys.: Condens. Matter **27**, 053203 (2015).

17 I. F. Mello, L. Squillante, G. O. Gomes, A. C. Seridonio, M. de Souza, J. Appl. Phys. **128**, 225102 (2020).

18 I. F. Mello, L. Squillante, G. O. Gomes, A. C. Seridonio, M. de Souza, Physica A **573**, 125963 (2021).